Effects of harmonic phase on nonlinear surface acoustic waves in the (111) plane of cubic crystals

R. E. Kumon[a] and M. F. Hamilton
Department of Mechanical Engineering, The University of Texas at Austin, Austin, Texas 78712-1063

(Received 11 February 2002; revised 5 October 2002; accepted 18 October 2002)

Spectral evolution equations are used to perform numerical studies of nonlinear surface acoustic waves in the (111) plane of several nonpiezoelectric cubic crystals. Nonlinearity matrix elements which describe the coupling of harmonic interactions are used to characterize velocity waveform distortion. In contrast to isotropic solids and the (001) plane of cubic crystals, the nonlinearity matrix elements usually cannot be written in a real-valued form. As a result, the harmonic components are not necessarily in phase, and dramatic variations in waveforms and propagation curves can be observed. Simulations are performed for initially monofrequency surface waves. In some directions the waveforms distort in a manner similar to nonlinear Rayleigh waves, while in other directions the velocity waveforms distort asymmetrically and the formation of shocks and cusped peaks is less distinct. In some cases, oscillations occur near the shocks and peaks because of phase differences between harmonics. A mathematical transformation based on the phase of the matrix elements is shown to provide a reasonable approximation of asymmetric waveform distortion in cases where the matrix elements have similar phase.
[DOI: 10.1121/1.1529170]

PACS numbers: 43.25.Fe, 43.35.Pt, 68.35.Iv, 62.65.+k [DEC]

I. INTRODUCTION

In a previous paper,[1] the authors used spectral evolution equations[2] to investigate the nonlinear propagation of surface acoustic waves (SAWs) in the (001) surface cut of nonpiezoelectric, cubic crystals. The present paper extends the analysis to nonlinear SAWs in the (111) surface cut. Results are presented for eight different crystals (KCl, NaCl, SrF_2, BaF_2, Si, Ge, Ni, and Cu) over the full range of propagation directions. In addition to the general study of these crystals, detailed studies are presented for the cases of silicon and potassium chloride in the (111) surface cut. In the case of silicon, some of the features described here have been corroborated by previously reported measurements.[3]

For isotropic media, the nonlinearity matrix in the spectral evolution equations has proven to be convenient both to interpret the nature of the spectral interactions[4] and to compute the shock formation distance.[5] In crystalline media, the nonlinearity matrix is especially useful for explaining the different types of waveform distortion that are possible as a result of the reduced symmetry. Unlike in previous theories for isotropic media[6] and for the (001) plane of cubic crystals,[1] the nonlinearity matrix elements in the (111) plane cannot usually be written in real-valued form. In particular, the phase of the nonlinearity matrix elements plays an important role in the resulting waveform distortion. A mathematical transformation is presented which gives reasonably accurate results for the distortion in cases where the phases of the first few nonlinearity matrix elements are similar. From this approach, a graphical table of various types of distortion can be constructed to estimate the nature of the distortion without solving the full system of nonlinear spectral evolution equations for every case.

II. NUMERICAL RESULTS

A. Linear effects

A plane surface wave with wave number k is assumed to propagate in the x direction along the surface of an anisotropic half-space $z \leqslant 0$. The displacement components of the linearized equations of motion can be written in the form [Eq. (22) in Ref. 2]

$$u_j = \sum_{s=1}^{3} C_s \alpha_j^{(s)} \exp[ikl_3^{(s)}] \exp[ik(x-ct)], \tag{1}$$

where $j = x,y,z$, c is the small-signal SAW speed, $l_3^{(s)}$ and $\alpha_j^{(s)}$ are the eigenvalues and eigenvectors, respectively, of the secular equation, and C_s are coefficients which allow the stress-free boundary conditions to be satisfied. The parameters c, $l_3^{(s)}$, $\alpha_j^{(s)}$, and C_s are determined using standard techniques.[7]

The SAW speed c as a function of the propagation direction in selected materials is shown in Fig. 1. These curves were computed using the same data as in Ref. 1. The direction of propagation is measured by the angle θ from the $\langle 11\bar{2} \rangle$ direction. The SAW speeds for each material are scaled by the characteristic speeds $c_{\text{ref}} = (c_{44}/\rho)^{1/2}$, where c_{ij} are the second-order elastic constants in Voigt notation and ρ is the density. The SAW speed is periodic every $\Delta\theta = 60°$ and symmetric about $\theta = 30°$. In most cases (and for all the cases shown here), the speeds group by anisotropy ratio $\eta = 2c_{44}/(c_{11}-c_{12})$, with materials possessing lower anisotropy ratios having higher relative SAW speeds. Materials with $\eta \approx 1$ indicate nearly isotropic media, with a corre-

[a]Current address: Department of Physics, University of Windsor, 401 Sunset Ave, Windsor, ON N9C 4E1, Canada. Electronic mail: kumon@mailaps.org

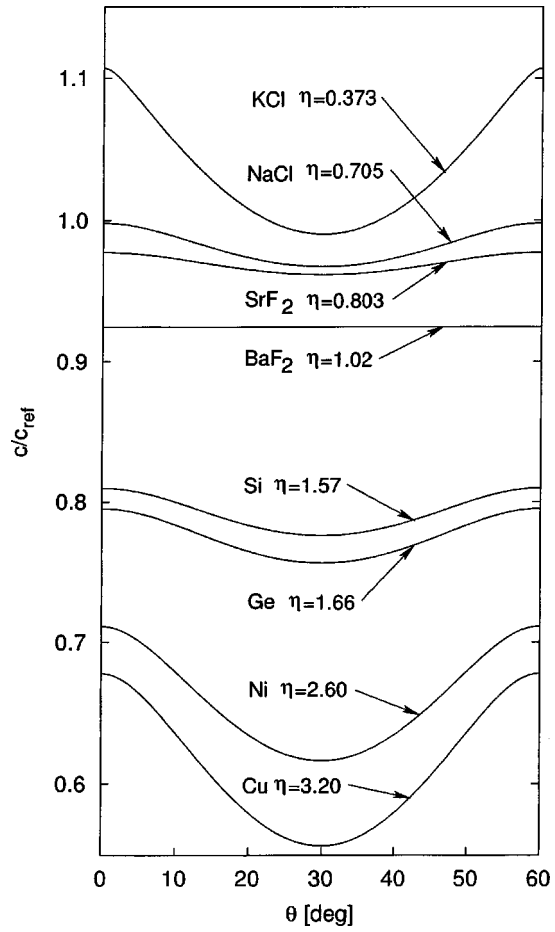

FIG. 1. SAW speed as a function of propagation direction in the (111) plane of selected materials. The SAW speed of each material is measured relative to $c_{\text{ref}}=(c_{44}/\rho)^{1/2}$, and the angle θ gives the direction of the wave vector relative to $\langle 11\bar{2}\rangle$. The wave speeds are periodic every $\Delta\theta=60°$.

spondingly constant SAW speed for all directions. For all materials, the directions $\theta=0°$, $\theta=30°$, and $\theta=60°$ are pure modes, i.e., the wave vector is parallel to the direction of power flow. As $\theta\rightarrow 30°$, the wave speed of the SAW mode tends to approach (but does not equal) the speed of one of the quasitransverse bulk wave modes, and the depth penetration penetration of the SAW mode tends to increase.[7] Unlike in the (001) plane the modes do not converge, and pseudo-surface wave modes do not exist in the direction $\theta=30°$.

While the wave speed has a sixfold periodicity in the (111) plane, other parameters of the linearized SAW equations have only a threefold periodicity.[8] For example, the eigenvalues $l_3^{(s)}$ have only a threefold symmetry. Figure 2 shows the real and imaginary parts of $l_3^{(s)}$ for KCl. (Compare with Fig. 16 in Ref. 7, which shows only $0°\leqslant\theta\leqslant 30°$.) One also finds that $|l_3^{(s)}|$ and $|C_s\alpha_j^{(s)}|$ exhibit a sixfold periodicity, while $\arg[l_3^{(s)}]$ and $\arg[C_s\alpha_j^{(s)}]$ maintain threefold periodicity. Because the nonlinearity matrix is a function of $l_3^{(s)}$ and $C_s\alpha_j^{(s)}$, this result also has implications for the periodicity of nonlinear effects, as discussed below.

B. Nonlinear effects

Because the nonlinear theory used here has been discussed at length elsewhere,[2] only the essential equations are summarized. The coupled nonlinear evolution equations for the surface acoustic waves (without absorption) are[2]

$$\frac{dv_n}{dx}=\frac{n^2\omega}{2\rho c^4}\sum_{l+m=n}\operatorname{sgn}(lm)S_{lm(-n)}v_l v_m, \tag{2}$$

where v_n is the spectral amplitude of the nth harmonic, $\omega=kc$ is the angular frequency, and S_{lm} is the nonlinearity

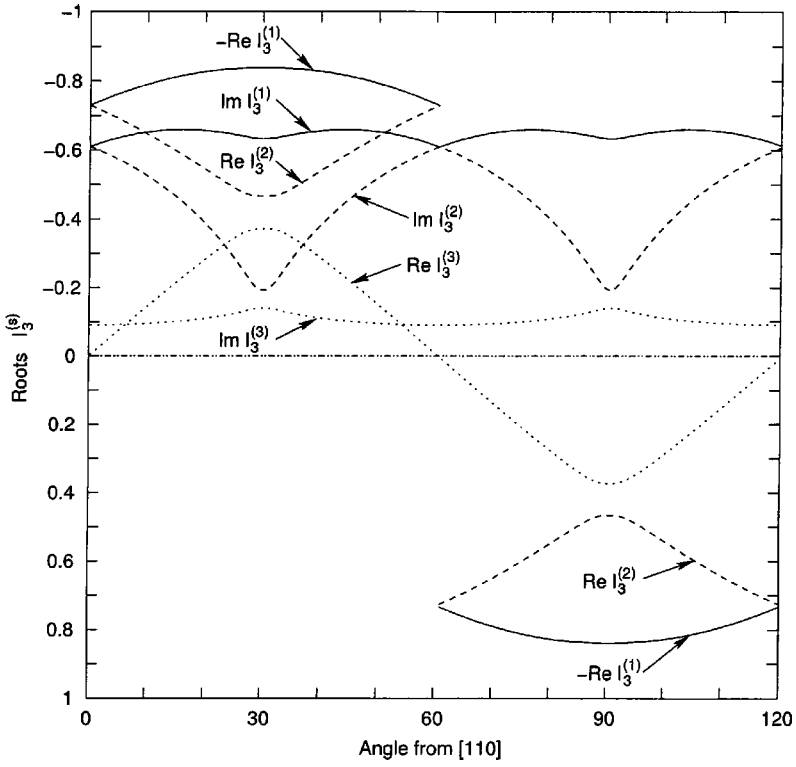

FIG. 2. Dependence of the eigenvalues $l_3^{(s)}$ on the direction of propagation for SAWs in the (111) plane of KCl (solid, long dashed, and short dashed lines for $s=1,2,3$, respectively). The figure is plotted such that it can be directly compared to Fig. 16 in Ref. 7, which only shows $0°\leqslant\theta\leqslant 30°$.

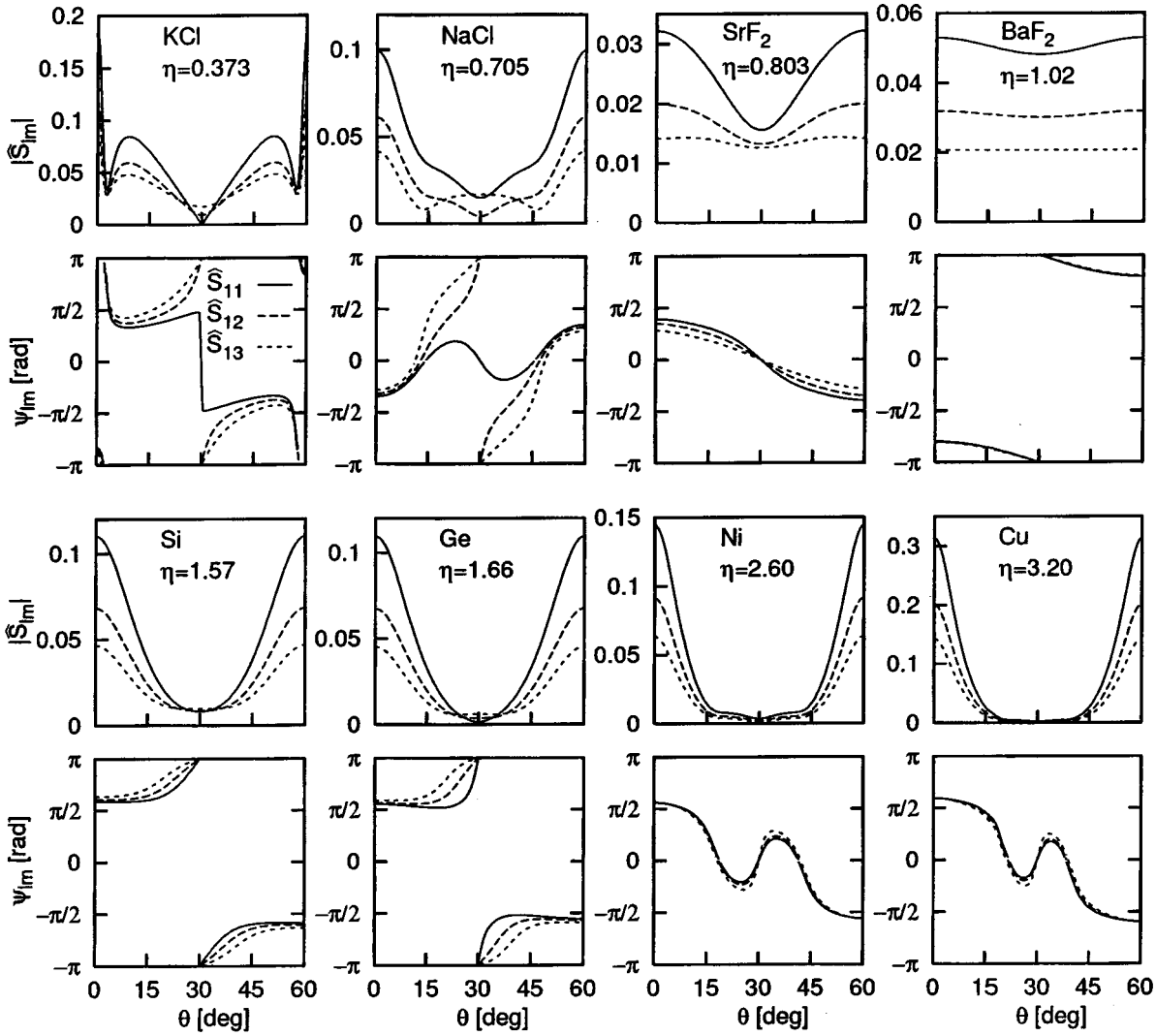

FIG. 3. Dependence of nonlinearity matrix elements on direction of propagation in the (111) plane for selected materials. The solid, long dashed, and short dashed lines correspond to $\hat{S}_{11}$, $\hat{S}_{12}$, and $\hat{S}_{13}$, respectively. The magnitudes $|\hat{S}_{lm}|$ of the matrix elements are plotted in the first and third rows, while the corresponding phases ψ_{lm} are plotted in the second and fourth rows.

matrix. The matrix element S_{lm} describes generation of the nth harmonic due to interaction of the lth and mth harmonics. The velocity waveforms at the surface ($z=0$) are computed from the spectral amplitudes by[1]

$$v_j(x,\tau)=\sum_n v_n(x)|B_j|e^{i\phi_j \operatorname{sgn} n}e^{-in\omega\tau}, \tag{3}$$

where $j=x,y,z$, $B_j=|B_j|\exp(i\phi_j)=C_s\alpha_j^{(s)}$ are determined by solving the linearized equations of motion, and $\tau=t-x/c$ is the retarded time. It is convenient to define a dimensionless nonlinearity matrix[1]

$$\hat{S}_{lm}=-S_{lm}/c_{44}. \tag{4}$$

In all cases, the figures throughout this paper use the nonlinearity matrix defined by Eq. (4).

It is possible that nonlinear coupling between surface wave and bulk wave modes may occur in propagation directions where the wave speeds in these modes are close to one another. The theoretical model does not account for coupling with bulk waves, and this matter was discussed previously in connection with Scholte waves.[9] Calculations have revealed that for the cases described in the present article, effects of mode coupling are negligible in most propagation directions for realistic wave amplitudes. Exceptions may include propagation directions in the region near $\theta=0°$ in Ni and Cu; care should be exercised in applying the aforementioned theory in these cases. A thorough analysis of this matter will be discussed in a future article.

1. General study

Figure 3 displays the nonlinearity matrix elements for KCl, NaCl, SrF_2, BaF_2, Si, Ge, Ni, and Cu. These are the same materials considered in Ref. 1 for the (001) surface cut. Plots for materials with $\eta<1$ or $\eta\approx1$ are given in the top two rows, and for materials with $\eta>1$ in the bottom two rows. Because the matrix elements are usually complex-valued, two plots are given for each material. The top plot in each pair shows the magnitudes $|\hat{S}_{11}|$ (solid), $|\hat{S}_{12}|$ (long dashed), and $|\hat{S}_{13}|$ (short dashed). The inequalities $|\hat{S}_{11}|>|\hat{S}_{12}|>|\hat{S}_{13}|$ hold in most directions within the crystals shown. In these cases, the primary effect of a change in

magnitude over a range of directions is to change the length scale over which the nonlinear distortion occurs. Exceptions occur when one or more of the matrix elements is zero[1] or when one or more of the above inequalities is reversed. The latter case occurs near $\theta=30°$ for KCl, NaCl, Si, and Ge (see Sec. II B 2 for the effect on the waveforms in Si). The matrix elements tend to decrease in magnitude as $\theta\rightarrow 30°$; this trend coincides with the increased depth penetration of the SAW described in Sec. II A. In all cases, the magnitudes $|S_{lm}|$ are periodic every $\Delta\theta=60°$ and symmetric about $\theta=30°$.

The phase ψ_{lm} of the matrix element $\hat{S}_{lm}$ is defined such that $\hat{S}_{lm}=|\hat{S}_{lm}|\exp(i\psi_{lm})$. The bottom plot in each pair shows the phases ψ_{11} (solid), ψ_{12} (long dashed), and ψ_{13} (short dashed). As will be shown in subsequent examples, the primary effect of the phase of the matrix elements is to change the shapes of the various velocity waveform components. Note that the nonlinearity matrix elements are always real-valued ($\psi_{lm}=0$ or $\psi_{lm}=\pm\pi$) at $\theta=30°$ because of the crystalline symmetry in this direction. In contrast to the magnitudes, the phases ψ_{lm} are periodic every $\Delta\theta=120°$ and symmetric about $\theta=60°$.

The nonlinearity matrix elements are functions of the parameters $l_3^{(s)}$ and $C_s\alpha_j^{(s)}$ of the linearized problem.[2] For the crystals shown (all in the $m\bar{3}m$ point group), the magnitudes $|S_{lm}|$, $|l_3^{(s)}|$, and $|C_s\alpha_j^{(s)}|$ have sixfold periodicity in the plane, while the phases $|\psi_{lm}|$, $\arg[l_3^{(s)}]$, and $\arg[C_s\alpha_j^{(s)}]$ have only threefold periodicity. Thus the symmetry properties of the nonlinearity matrix elements are influenced by the symmetry properties of these linear parameters.

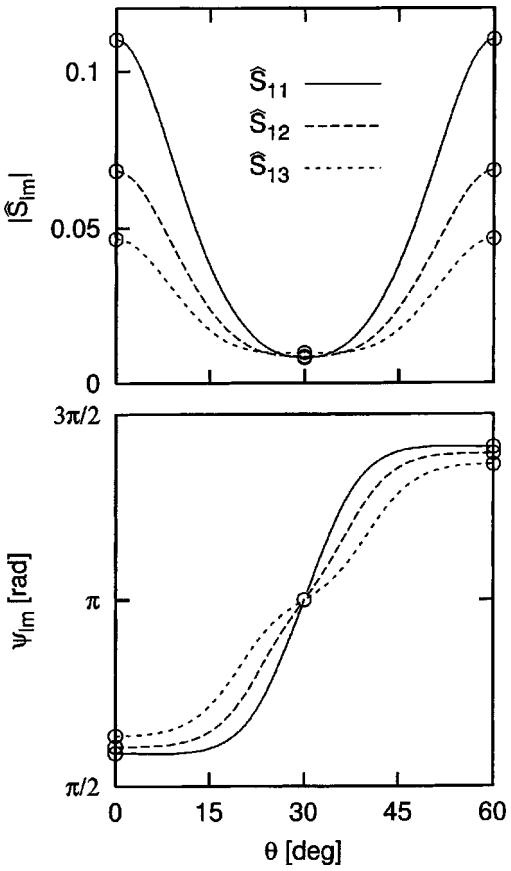

FIG. 4. Nonlinearity matrix elements $\hat{S}_{11}$, $\hat{S}_{12}$, and $\hat{S}_{13}$ for Si in the (111) plane as a function of direction for $0°\leqslant\theta\leqslant 60°$. The circled directions are discussed in detail in the text. Note that the vertical scale on the phase graph is changed to $\pi/2\leqslant\psi_{lm}\leqslant 3\pi/2$ as compared to Fig. 3.

2. Detailed study of silicon

Here we consider nonlinear SAWs in crystalline silicon and show some of the various types of waveform distortion which are possible. Figure 4 (expanded from Fig. 3 with the vertical scale of the phase changed to $\pi/2\leqslant\psi_{lm}\leqslant 3\pi/2$) shows the magnitude and phase of the three nonlinearity matrix elements $\hat{S}_{11}$ (solid), $\hat{S}_{12}$ (long dashed), and $\hat{S}_{13}$ (short dashed). While $\theta=0°$, $\theta=30°$, $\theta=60°$ are pure mode directions, none is a "Rayleigh-type" mode.[7] In the $\theta=0°$ and $\theta=60°$ cases, while the displacement is confined to the sagittal plane, the phase difference between the longitudinal and vertical components is not 90°. Hence the major axis of the initial surface displacement ellipse is not perpendicular to the surface. In the $\theta=30°$ case, the displacement is not confined to the sagittal plane.

Figure 5 displays the velocity waveforms for the directions $\theta=0°$, $\theta=30°$, and $\theta=60°$ marked by small circles in Fig. 4. These waveforms were calculated under the same conditions as described in Ref. 1 and are selected to show the types and diversity of distortion in this cut. The columns from left to right give the dimensionless longitudinal (V_x), transverse (V_y), and vertical (V_z) components of the velocity, respectively. In each direction, the waveforms are normalized such that at $X=0$ we have $|V_x|^2+|V_y|^2+|V_z|^2=1$, and hence the absolute magnitudes between directions should not be compared. The velocity waveforms show results at locations $X=x/x_0=0$ (short dashed), $X=1$ (long dashed), and $X=2$ (solid), where $x_0=\rho c^4/4|S_{11}|\omega v_0$ is a characteristic length scale for nonlinear distortion (approximately equal to the shock formation distance, if shocks form)[1] and v_0 is a characteristic velocity magnitude.

$\theta=0°$: This direction provides the first example of asymmetric distortion. While the velocity waveforms are symmetric about $\omega\tau=0$ at $X=0$, the distortion is asymmetric at $X=1$ and $X=2$, unlike both nonlinear Rayleigh waves[6] and nonlinear SAWs in the (001) plane.[1] For example, a nonlinear Rayleigh wave forms a cusped sawtooth wave with a compression or rarefaction shock in the V_x waveform and a U-shaped wave with a cusped peak in the V_z waveform. However, in this direction the V_x waveform distorts into a U-shaped wave with an asymmetrically cusped peak, while the V_z waveform distorts into a sawtoothlike wave with peaks advancing and troughs receding with respect to the retarded time frame. Measurements of finite-amplitude SAWs at $\theta=0°$ in Si corroborate these results.[3] The source of these differences is the complex-valued nature of the nonlinearity matrix elements. Because a full discussion of the relationship between the phase of the matrix elements and the resulting waveform distortion is given in Sec. III, further analysis of these waveforms is delayed until Sec. IV.

$\theta=30°$: In this direction, the nonlinearity matrix elements are all real-valued. As a result, the distortion is

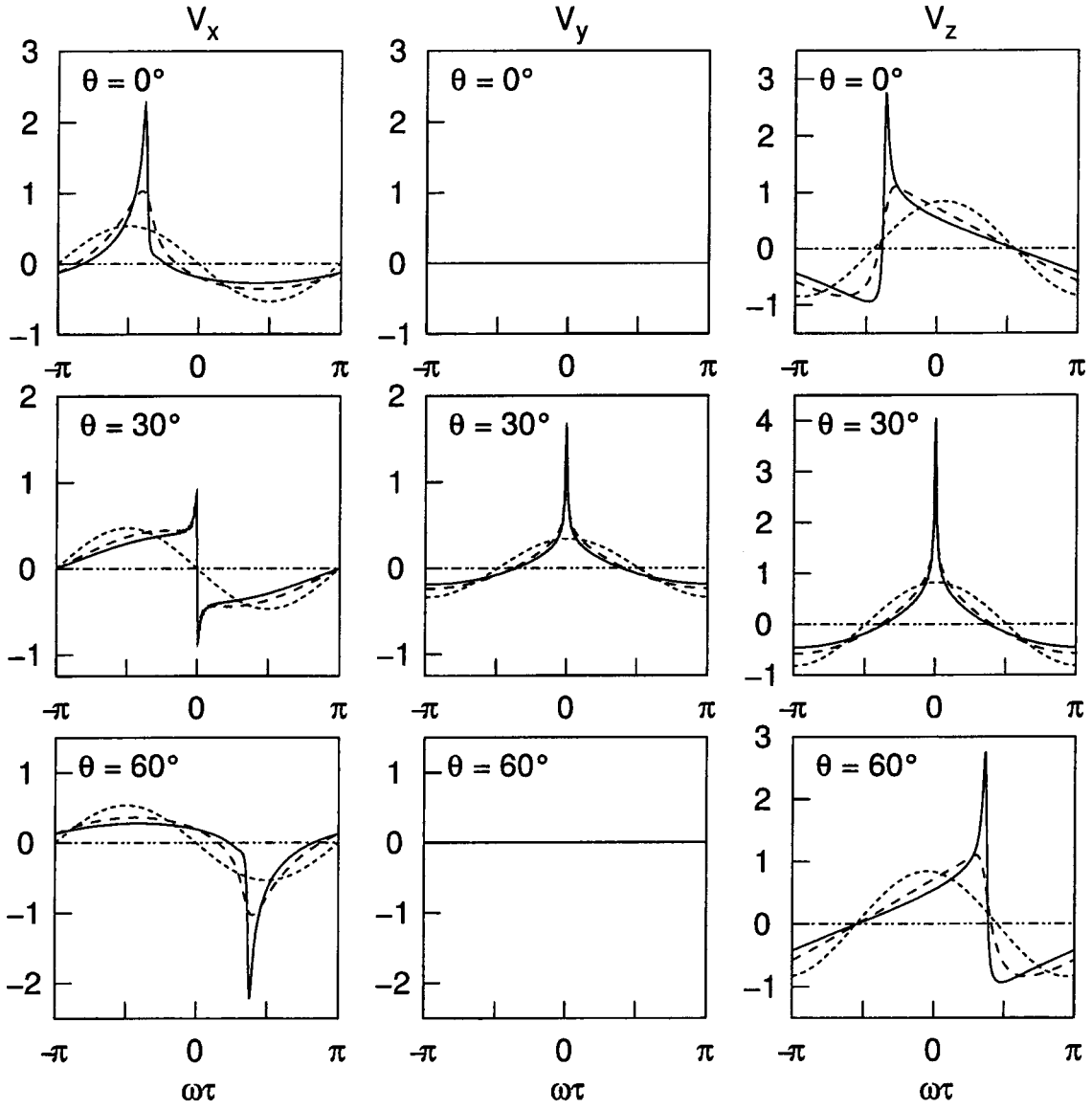

FIG. 5. Velocity waveforms in selected directions for propagation in the (111) plane of Si. The velocity components are normalized such that initial amplitude satisfies $|V_x|^2+|V_y|^2+|V_z|^2=1$ in each propagation direction. The short dashed, long dashed, and solid lines correspond to propagation at distances $X=0$, $X=1$, and $X=2$, respectively.

more similar to nonlinear SAWs in certain directions of the (001) plane.[1] Because $|S_{11}|$ is less than $|S_{12}|$ and $|S_{13}|$, energy is more efficiently transferred from the fundamental to third and higher harmonics than it is to the second harmonic. As a result of the increased energy in the higher harmonics, the velocity waveforms show sharp cusps. In addition, the matrix elements are negative ($\psi_{lm}=\pi$), and so a rarefaction shock forms in the V_x waveform.

$\theta=60°$: While the nonlinearity matrix elements in this direction have the same magnitude as those for $\theta=0°$, their phases have the opposite sign. As a result, the waveforms distort into entirely different shapes. The V_x waveform distorts into an inverted U-shaped wave with an asymmetrically cusped trough, while the V_z waveform distorts into an asymmetric sawtoothlike wave with peaks receding and troughs advancing. Because the nonlinear properties are periodic every $\Delta\theta=120°$, propagation for $\theta=60°$ is the same as for $\theta=180°$. Recently reported measurements[8] have shown that nonlinear propagation is different for $[11\bar{2}]$ and $[\bar{1}\bar{1}2]$ in the (111) plane of crystalline silicon, and the differences in the distortion are consistent with the results shown here.

3. Detailed study of potassium chloride

We consider here nonlinear SAWs in the (111) plane of KCl. The magnitude and phase of $\hat{S}_{11}$ (solid), $\hat{S}_{12}$ (long dashed), and $\hat{S}_{13}$ (short dashed) are shown in Fig. 6 (expanded from Fig. 3 for $0°\leqslant\theta\leqslant30°$ and with the vertical scale of the phase changed to $0\leqslant\psi_{lm}\leqslant3\pi/2$). Like Si, the nonlinearity matrix elements have the largest magnitude at $\theta=0°$. Unlike Si, the phases ψ_{lm} change significantly from $\theta=0°$ to 5°. Here again both the $\theta=0°$ and $\theta=30°$ directions are pure mode directions, but neither is a ''Rayleigh-type'' mode for the same reasons as in Si. One marked difference with Si which occurs even at linear order is that the transverse linear amplitude factors B_y have phases ϕ_y that are

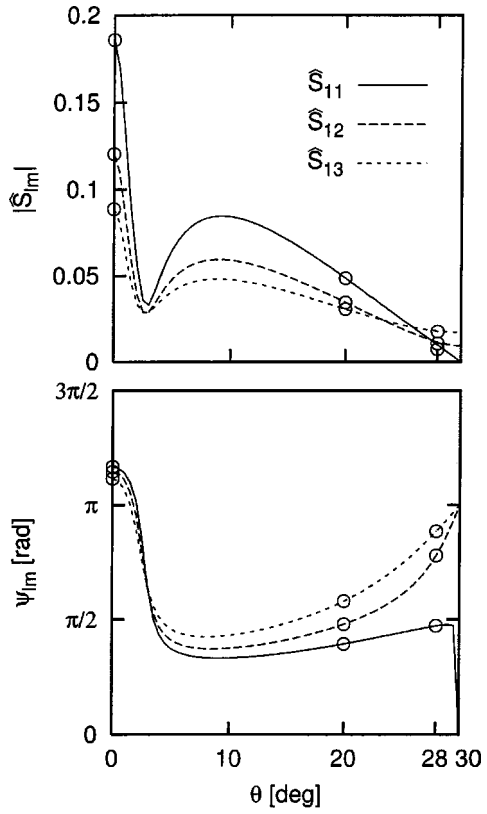

FIG. 6. Nonlinearity matrix elements $\hat{S}_{11}$, $\hat{S}_{12}$, and $\hat{S}_{13}$ for KCl in the (111) plane as a function of direction for $0° \leqslant \theta \leqslant 30°$. The circled directions are discussed in detail in the text. Note that the vertical scale on the phase graph is changed to $0 \leqslant \psi_{lm} \leqslant 3\pi/2$ as compared to Fig. 3.

closer to π than to 0. This change alone results in transverse velocity waveforms that are significantly different.

Figures 7 and 8 display the velocity waveforms and harmonic propagation curves, respectively, for the directions $\theta = 0°$, $\theta = 20°$, and $\theta = 28°$ marked by small circles in Fig. 6. These directions are chosen because they have types of waveform distortion not shown in Fig. 5. Note that the vertical axis for all the waveforms is shifted as compared to Fig. 5 such that $0 \leqslant \omega\tau \leqslant 2\pi$. The harmonic propagation curves show the spectral components V_1 to V_5 as a function of the dimensionless propagation distance. Because the spectral amplitudes are complex-valued, the harmonic propagation curves show both the magnitudes (left column) and phases (right column) of the harmonics. Note that the phases shown are relative to linear theory.

$\theta = 0°$: This direction shows a different type of asymmetric distortion than seen in Si. The V_x waveform forms an asymmetrically cusped sawtoothlike wave with a rarefaction shock and with the negative cusped peak larger in magnitude than the positive cusped peak. The V_z waveform forms a U-shaped wave with an asymmetrically cusped peak. The harmonic magnitude curves in Fig. 8 are typical of nonlinear SAWs in isotropic solids, and the harmonic phase curves show relatively little variation during propagation.

$\theta = 20°$: Observe that the waveforms in this direction distort very differently from those in the $\theta = 0°$ direction. The different shapes result because the dominant nonlinearity matrix elements are clustered near $\pi/2$, instead of near π like at $\theta = 0°$ (see Fig. 6). Moreover, the phases of ψ_{11}, ψ_{12}, and ψ_{13} are more widely spaced at $\theta = 20°$ than at $\theta = 0°$.

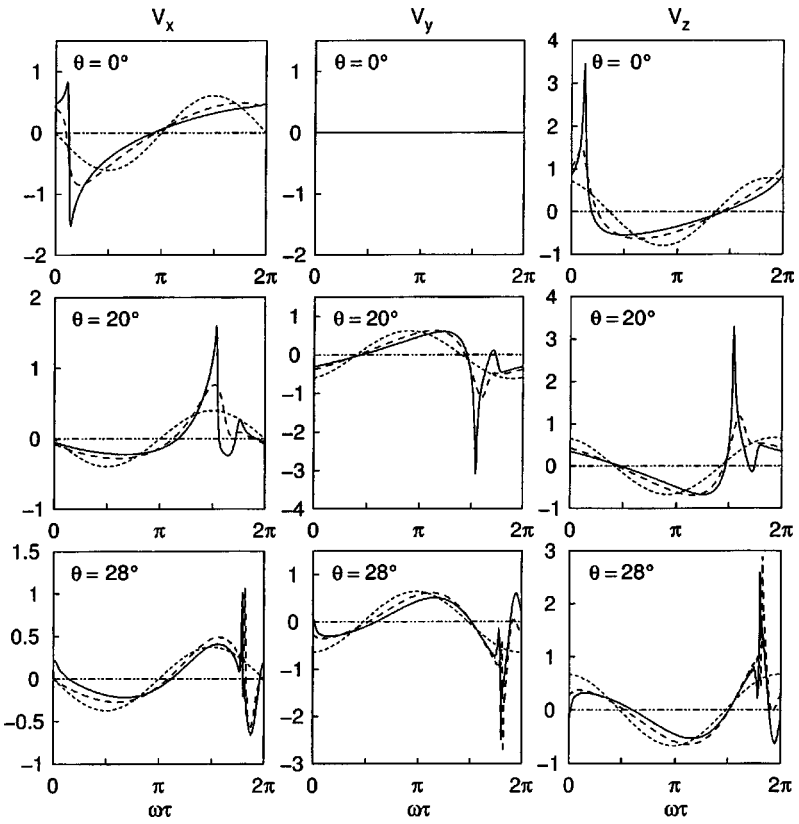

FIG. 7. Velocity waveforms in selected directions of propagation in the (111) plane of KCl. The velocity components are normalized such that initial amplitude satisfies $|V_x|^2 + |V_y|^2 + |V_z|^2 = 1$ in each propagation direction. The short dashed, long dashed, and solid lines correspond to propagation at distances $X = 0$, $X = 1$, and $X = 2$, respectively.

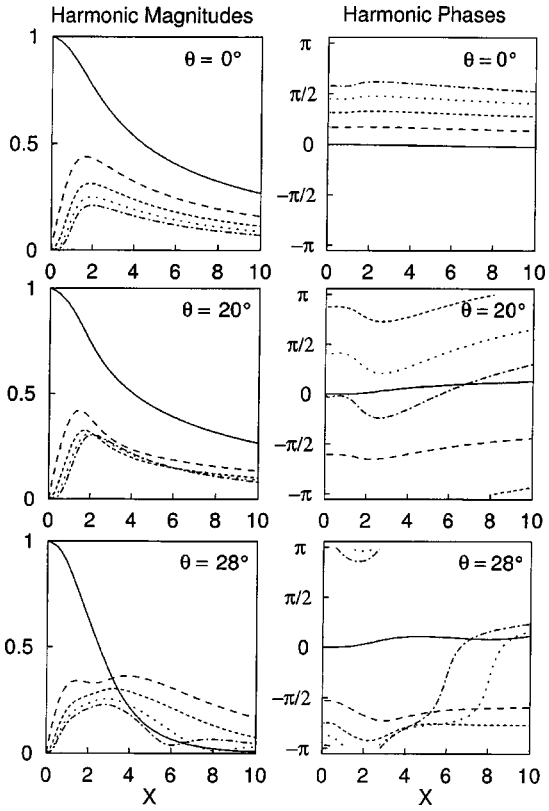

FIG. 8. Harmonic propagation curves for selected directions of propagation in the (111) plane of KCl. The spectral components V_1 (solid), V_2 (long dashed), V_3, (short dashed), V_4 (dotted), and V_5 (dot-dashed) are plotted as a function of distance. The left column shows the spectral amplitudes $|V_n|$, while the right column shows the spectral phases arg V_n relative to linear theory.

This separation causes the oscillations near the shocks and peaks, as discussed further in Sec. IV. While these oscillations are reminiscent of the kind seen in dispersive waves, it should be emphasized that there is no dispersion in this system. In contrast to the $\theta=0°$ direction of KCl, Fig. 8 shows that the magnitudes of the third, fourth, and fifth harmonics become comparable, while the phases are further separated and show larger variation as a function of distance except at the fundamental frequency.

$\theta=28°$: In this direction, $|\hat{S}_{11}|$ is less than $|\hat{S}_{12}|$ and $|\hat{S}_{13}|$, similar to the $\theta=30°$ direction in Si. Energy in the fundamental is thus converted more rapidly to higher harmonics. As shown in Fig. 8, this results in a steeper decline in the magnitude of the fundamental as compared to the previous two directions in KCl, and eventual dominance by the higher harmonics. However, unlike Si, here the phases of the nonlinearity elements are different. Figure 8 shows that the harmonic phases are irregularly spaced and some harmonics change their phase significantly as they propagate. The net result of these complicated interactions is the high-frequency oscillation seen in the waveforms of Fig. 6.

These simulations show that a wide variety of waveform distortion can occur in nonlinear SAWs in the (111) plane as compared to nonlinear Rayleigh waves or nonlinear SAWs in the (001) plane. Features like asymmetric distortion and high-frequency oscillations in the waveforms result from the harmonics having dissimilar phases, which in turn are related to the complex-valued nature of the matrix elements. The next section further investigates the relationship between the nonlinearity matrix elements and waveform distortion.

III. COMPLEX-VALUED NONLINEARITY MATRIX ELEMENTS AND WAVEFORM DISTORTION

Only the concepts of positive and negative nonlinearity are necessary to describe nonlinear SAWs in the (001) plane.[1] Examples of waves with a positive coefficient of nonlinearity β include acoustic waves in fluids, longitudinal bulk waves in most isotropic solids, and SAWs in steel[10] and the direction 26° from ⟨100⟩ in Si.[1] In these waves, the peaks of the longitudinal velocity waveforms advance in a retarded time frame moving at the linear wave speed, while the troughs recede. Examples of waves with $\beta<0$ include SAWs in fused quartz[11] and SAWs propagating in the directions 0° and 35° from ⟨100⟩ in the (001) plane of Si.[1] In these waves, the peaks of the longitudinal velocity waveforms recede in the retarded time while the troughs advance. However, the situation is more complicated for the most general case of a SAW in an anisotropic medium. As shown in Ref. 1, an appropriate coefficient of nonlinearity for SAWs in a crystal is

$$\beta=4c_{44}\hat{S}_{11}/\rho c^2, \tag{5}$$

where the nonlinearity matrix element $\hat{S}_{11}=|\hat{S}_{11}|\exp(i\psi_{11})$ cannot usually be written in real-valued form. The interpretation of Eq. (5) in terms of its effect on waveforms for situations other than $\psi_{11}=0$ (β real and positive) and $\psi_{11}=\pm\pi$ (β real and negative) is not immediately obvious. The purpose of this section is to suggest a way of thinking about this issue.

Ideally, one would like to be able to characterize the type of waveform distortion by computing just a few parameters, thereby avoiding the process of numerically integrating a system of nonlinear differential equations for every material, cut, and direction. As shown in Ref. 1, the nonlinearity matrix elements can serve as such parameters, allowing a reasonable estimate of the type of waveform distortion (or lack thereof) to be determined from plots of the first few elements. The ability to make the same type of estimate is desired here. The specific objective is to investigate in a simplified manner how the phase of the nonlinearity matrix affects the SAW solutions.

Towards this end, the matrix

$$S_{lm}^{\psi}=S_{lm}e^{i\psi\,\mathrm{sgn}\,n} \tag{6}$$

is introduced to represent a nonlinearity matrix constructed by applying a phase increment ψ, independent of l and m, to a given matrix S_{lm}. Given a solution for a material with matrix S_{lm}, it is desired to relate that solution to the one obtained for a material with nonlinearity matrix S_{lm}^{ψ}. It is convenient, although not necessary, to consider the matrix

S_{lm} to be real. The main simplifying assumption is that there exist propagation directions in some materials for which the phase of the nonlinearity matrix is nonzero yet independent of the indices l and m. That Eq. (6) is a reasonable model of the phase dependence in some cases, at least for the first few matrix elements, is supported by Fig. 3. Specifically, one observes that $\psi_{11} \simeq \psi_{12} \simeq \psi_{13}$ for all the materials shown (except SrF_2) at $0° < \theta < 15°$ and $45° < \theta < 60°$. The purpose of introducing $\operatorname{sgn} n$ in Eq. (6) is that S_{lm}^{ψ} must retain all the symmetry properties required of the nonlinearity matrix. In particular, the nonlinearity matrix elements have the symmetry property[2]

$$S_{lm(-n)} = S^*_{(-l)(-m)n}, \tag{7}$$

where $n = l + m$. The $\operatorname{sgn} n$ ensures that Eq. (6) satisfies Eq. (7).

For a nonlinearity matrix S_{lm}^{ψ}, the evolution of nonlinear SAWs is described by Eqs. (2):

$$\frac{dv_n^{\psi}}{dx} = \frac{n^2\omega_0}{2\rho c^4} \sum_{l+m=n} \operatorname{sgn}(lm) S_{lm(-n)}^{\psi} v_l^{\psi} v_m^{\psi}, \tag{8}$$

where the notation v_n^{ψ} designates that these spectral components are the solutions associated with the matrix S_{lm}^{ψ}. Now substitute Eq. (6) into Eq. (8) and multiply both sides by $e^{i\psi \operatorname{sgn} n}$. Let

$$v_n = v_n^{\psi} e^{i\psi \operatorname{sgn} n}, \tag{9}$$

and thus obtain

$$\frac{dv_n}{dx} = \frac{n^2\omega_0}{2\rho c^4} \sum_{l+m=n} \operatorname{sgn}(lm) S_{lm(-n)} v_l v_m. \tag{10}$$

The spectral components v_n in Eq. (10) are recognized as the solutions for a material with nonlinearity matrix S_{lm}. Therefore, the solutions v_n^{ψ} for a material with nonlinearity matrix S_{lm}^{ψ} are related to the solutions v_n for a material with nonlinearity matrix S_{lm} via Eq. (9):

$$v_n^{\psi} = v_n e^{-i\psi \operatorname{sgn} n}. \tag{11}$$

The surface velocity components v_j^{ψ} in the x_j direction for a material with nonlinearity matrix S_{lm}^{ψ} are reconstructed from the spectral components v_n^{ψ} using Eq. (3):

$$v_j^{\psi}(x,\tau) = \sum_n v_n^{\psi}(x) |B_j| e^{i\phi_j \operatorname{sgn} n} e^{-in\omega_0\tau}. \tag{12}$$

For ease of notation, define $\hat{S}_{lm}^{\psi} = -S_{lm}^{\psi}/c_{44}$, following Eq. (4).

Consider an example of the above procedure to relate the phase of the nonlinearity matrix elements to the corresponding type of waveform distortion. Take the well-known waveform distortion for a nonlinear Rayleigh wave with positive nonlinearity coefficient β as a reference case, with spectrum v_n^R, corresponding real-valued nonlinearity matrix elements $\hat{S}_{lm}^R$, and $B_x^R = |B_x^R| e^{-i\pi/2} = -i|B_x^R|$ (this convention for B_j is chosen to be consistent with theory for nonlinear Rayleigh waves in isotropic solids[6]). For simplicity, we consider only the longitudinal velocity waveforms. The longitudinal velocity waveform for the nonlinear Rayleigh wave is given by

$$v_x^R(x,\tau) = \sum_n v_n^R(x)(-i|B_x^R| \operatorname{sgn} n) e^{-in\omega_0\tau}. \tag{13}$$

Now suppose there exists a hypothetical crystal with nonlinearity matrix elements $\hat{S}_{lm}^{\psi} = \hat{S}_{lm}^R e^{i\psi \operatorname{sgn} n}$ and linear amplitude factors $B_x = |B_x| e^{-i\pi/2} = -i|B_x|$. By Eq. (12), the longitudinal velocity waveform at the surface of the crystal is written in terms of the spectral components of the Rayleigh wave as

$$v_x^{\psi}(x,\tau) = \sum_n v_n^{\psi}(x)(-i|B_x| \operatorname{sgn} n) e^{-in\omega_0\tau}, \tag{14}$$

or, from Eq. (11),

$$v_x^{\psi}(x,\tau) = \frac{|B_x|}{|B_x^R|} \sum_n v_n^R(x) e^{-i\psi \operatorname{sgn} n}(-i|B_x^R| \operatorname{sgn} n) e^{-in\omega_0\tau}. \tag{15}$$

Except for the factor of $e^{-i\psi \operatorname{sgn} n}$, the summation is the longitudinal velocity component of the Rayleigh wave. The prefactor $|B_x|/|B_x^R|$ adjusts for possible amplitude differences between the linear solutions of the Rayleigh wave and the SAW in the crystal. Thus, given the linear amplitude factor B_x and the phase ψ of the nonlinearity matrix elements, the waveforms at the surface in the idealized crystal may be computed by changing the phase of the spectral components of the nonlinear Rayleigh wave and reconstructing according to Eq. (15).

The expression in Eq. (15) is only an approximation to the actual waveform. Discrepancies occur because the nonlinearity matrix elements rarely possess identical phase and, even if the phases of the elements are very similar, the magnitudes of the elements may differ. Nevertheless, the overall result can be qualitatively similar, especially in cases where the dominant matrix elements have nearly the same phase.

To gain some intuition about the example transformation $v_n^{\psi} = v_n e^{-i\psi \operatorname{sgn} n}$ given in Eq. (15), the dimensionless waveforms

$$V_x^{\psi}(x,\tau) = \frac{v_x^{\psi}(x,\tau)}{|v_x^{\psi}(0,0)|} = \sum_n v_n^R(x)(-i \operatorname{sgn} n) e^{-i\psi \operatorname{sgn} n} e^{-in\omega_0\tau} \tag{16}$$

are plotted in Fig. 9 for $0 \leqslant \psi \leqslant \pi$. (An analogous figure[12] can be constructed $-\pi \leqslant \psi \leqslant 0$.) The Rayleigh waveforms ($\psi = 0$) are calculated for steel. The third-order elastic constants for the simulations are taken from measurements of "Steel 60 C2H2A" listed in the review by Zarembo and Krasil'nikov,[13] and they are the same as those used in simulations by Zabolotskaya[6] and Shull *et al.*[10] The simulations were performed under conditions identical to the crystal simulations described in Ref. 1. Each plot contains the dimensionless longitudinal velocity waveforms $V_x^{\psi}(X)$ at locations $X = 0$ (short dashed), $X = 1$ (long dashed), and $X = 2$ (solid).

Several observations can be made about this table of graphs. In the limiting cases of $\psi = 0$ and $\psi = \pi$, the waveforms distort positively and negatively, respectively. When

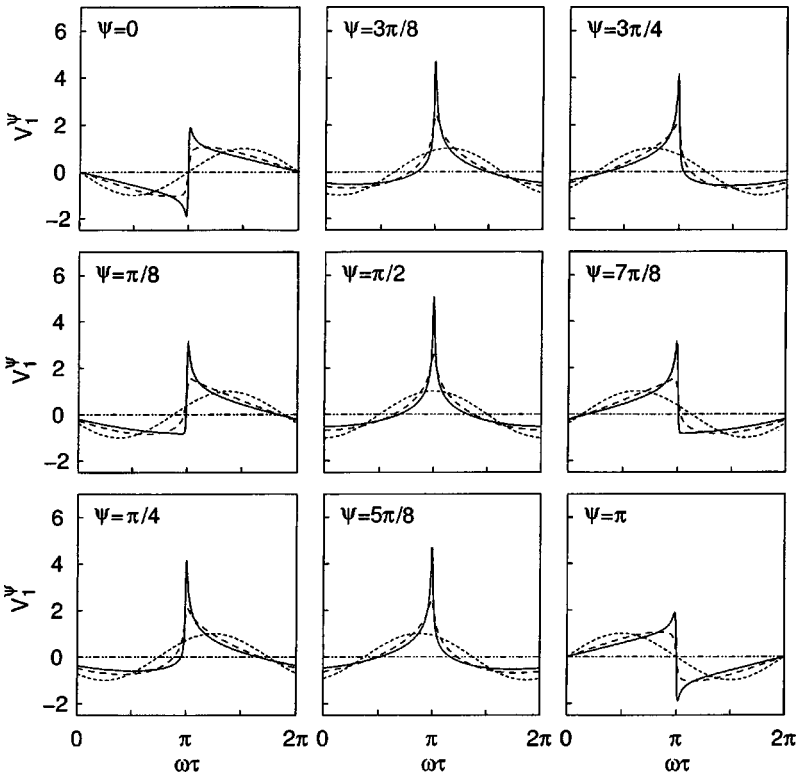

FIG. 9. Transformed waveforms corresponding to the various phase angles $0 \leqslant \psi \leqslant \pi$ of the transformed nonlinearity matrix elements $\hat{S}_{lm}^{\psi} = \hat{S}_{lm} e^{i\psi \operatorname{sgn} n}$, where $n = l + m$. Each graph plots the dimensionless longitudinal velocity waveforms $V_x^{\psi}(x,\tau) = v_x^{\psi}(x,\tau)/|v_x^{\psi}(0,0)|$ for waveforms at distances $X=0$ (short dashed), $X=1$ (long dashed), $X=2$ (solid).

$\psi = \pi/2$, the waveform looks like the vertical velocity component of a negatively distorting Rayleigh wave. This similarity occurs because, from Eq. (11),

$$v_n^{\psi=\pi/2} = v_n e^{-i(\operatorname{sgn} n)\pi/2} = (-i \operatorname{sgn} n) v_n, \tag{17}$$

where the coefficient $-i \operatorname{sgn} n$ is recognized as a Hilbert transform expressed in the frequency domain.[14] The appearance of the Hilbert transform in Eq. (17) is not unexpected because the longitudinal and vertical components of a Rayleigh wave are related in precisely this way. The remaining plots show the expected waveform shapes for intermediate values of ψ and, therefore, other cases of complex-valued nonlinearity matrix elements.

This approximate approach is not limited to longitudinal velocity waveforms. If the phases ϕ_j of the linear amplitude factors B_j are known, then the corresponding approximate waveform distortion in the vertical and transverse directions can also be determined. Let $\psi_{\text{long}} = \psi_{lm}$ be the phase of all the matrix elements. In cases where the phases are not all the same, choose a representative element, typically ψ_{11}. The appropriate values of ψ_{tran} and ψ_{vert} used to characterize the transverse and vertical velocity waveforms are given by[12]

$$\psi_{\text{tran}} = \phi_1 - \phi_2 + \psi_{\text{long}}, \tag{18a}$$

$$\psi_{\text{vert}} = \phi_1 - \phi_3 + \psi_{\text{long}}. \tag{18b}$$

In other words, these are the phases that are appropriate to use with Eq. (12) and Fig. 9 (and its analog for $-\pi \leqslant \psi \leqslant 0$) to determine the approximate shape of the waveform distortion. Calculated phase values using Eqs. (18) for the directions and crystals discussed in this paper are given in Ref. 12.

IV. COMPARISON OF APPROXIMATE AND FULL SOLUTION METHODS

Figure 10 shows comparisons of the transformed solutions based on nonlinear Rayleigh waves in steel and the solutions for the distortion of longitudinal waveforms in several real crystals. The transformed solutions based on Rayleigh waves are constructed via Eq. (12) in three steps. First, the linear amplitude factor B_x and nonlinearity matrix element $\hat{S}_{11}$ are computed for each crystal. Second, the transformation v_n^{ψ} in Eq. (11) is applied to the spectral components v_n^R of the nonlinear Rayleigh waves using ψ_{11}, and the waveforms are translated so that all the sine waves at the source begin in the same place on the horizontal scale. Third, the resulting waveforms are scaled using $|B_x|$ such that the amplitude of the undistorted waveform at $X=0$ is equal in magnitude to the waveform in the corresponding crystal. The left column gives the transformed Rayleigh wave solutions, while the right column gives the simulations using the full theory (reproduced from Figs. 5 and 7). The rows present comparisons for waveforms propagating in the directions $\theta = 0°$ for Si and $\theta = 0°$, $\theta = 20°$, and $\theta = 28°$ for KCl.

The top two rows show cases for which the nonlinearity elements $\hat{S}_{11}$, $\hat{S}_{12}$, and $\hat{S}_{13}$ have similar, but not the same, phase. For $\theta = 0°$ in Si the characteristic phase was chosen as $\psi_{\text{long}} = \psi_{11} \approx 0.59\pi$ (see Fig. 4). Thus for this case the waveform is expected to be between the shapes given by $\psi = \pi/2$ and $\psi = 5\pi/8$ in Fig. 9. Similarly, the characteristic phase for $\theta = 0°$ in KCl was chosen to be $\psi_{\text{long}} = \psi_{11} \simeq 1.17\pi$ (see Fig. 6). The transformed Rayleigh wave solutions reproduce the general shape of the distortion although not all the details. For example, in the Si waveform the shock

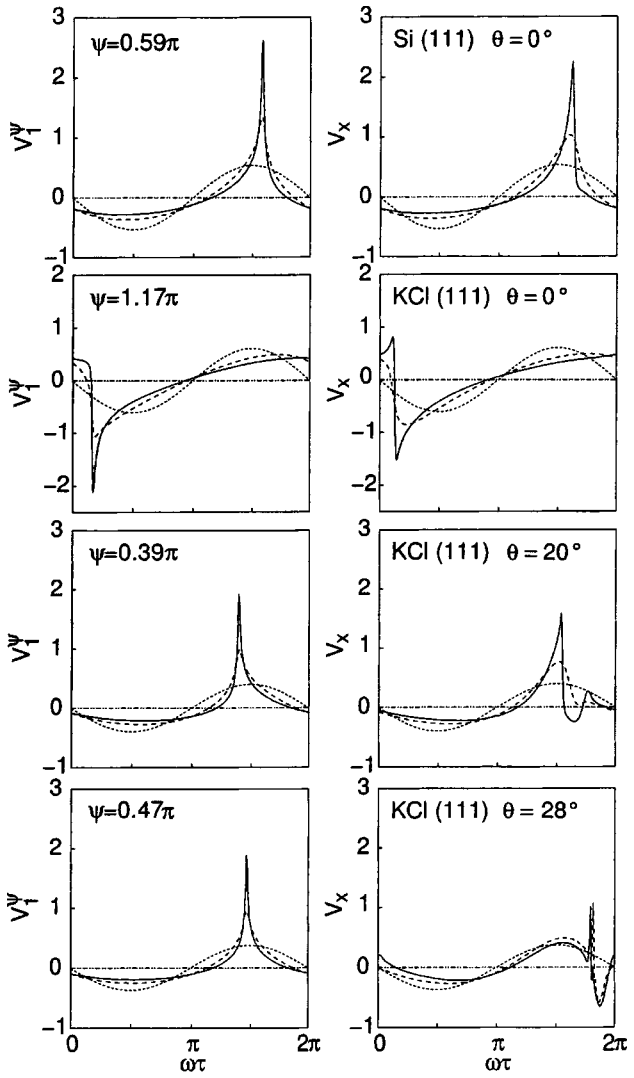

FIG. 10. Comparison of transformed Rayleigh wave solutions (left column) and simulations of nonlinear SAWs in the direction $\theta=0°$ for Si and the directions $\theta=0°$, $\theta=20°$, and $\theta=28°$ for KCl (right column). The top two rows correspond to cases of nonlinearity matrix elements with similar phase, while the bottom two rows show cases where the matrix elements have dissimilar phase.

is steeper than in the transformed waveform, and in the KCl waveform the cusping before the shock does not appear in the transformed waveform. Nevertheless, the similarities between the waveforms are striking. In cases like these, the nonlinearity matrix elements and plots like Fig. 9 can be used to immediately characterize the nature of the waveform distortion.

In contrast, the bottom two rows show several cases where the phases of the nonlinearity matrix elements are less similar. At $\theta=20°$ in KCl, the characteristic phase for the approximate method was chosen to be $\psi_{\text{long}}=\psi_{11}\simeq 0.39\pi$. In this case, the approximately transformed waveforms do not reproduce the extra oscillations that result from the the phase differences introduced between harmonics during the harmonic generation process. However, the occurrence of the oscillations to the right of the cusped peak can be inferred from the relation $\psi_{11}<\psi_{12}<\psi_{13}$. As higher harmonics form, their phase relative to the fundamental is increased. Additional calculations of velocity waveforms in the (111) plane of Ni, where $\psi_{11}>\psi_{12}>\psi_{13}$ (see Fig. 3), correspondingly show that oscillations appear to the left of the peaks and shocks in those waveforms.[12] At $\theta=28°$ in KCl, the characteristic phase for the transformed waveforms was chosen to be $\psi_{\text{long}}=\psi_{11}\simeq 0.47\pi$. However, the approximate method does not reproduce the features seen in the full simulation. This is not unexpected because, as seen in Fig. 6, $|\hat{S}_{11}|<|\hat{S}_{12}|<|\hat{S}_{13}|$, and thus $\hat{S}_{11}$ does not dominate the distortion process. In addition, ψ_{11} differs significantly from ψ_{12} and ψ_{13} in this direction. Under these circumstances, the approximate method is not likely to reproduce all the salient features of the distortion. However, this determination can be made directly by examining a plot of the nonlinearity matrix elements.

Finally, the methods and results described in this paper are not limited to nonlinear SAWs in the (111) surface cut. Additional studies of a variety of cubic crystals in the (110) surface cut have been performed.[12] While the waveform distortion in this cut is similar to that in the (001) plane for crystals in the $m\bar{3}m$ point symmetry group[15] (all the crystals shown in this paper), crystals in the $m\bar{3}$ point group show distortion like in the (111) plane. Examples of crystals in the $m\bar{3}$ point group are the hydrous alums $X\text{Al}(\text{SO}_4)_2\cdot 12\text{H}_2\text{O}$, where $X=$Cs, K, and NH_4. The use of complex-valued nonlinearity matrix elements to characterize waveform distortion is also expected to be applicable to surface waves in materials with other crystalline symmetries besides cubic.

V. SUMMARY

This paper examines the propagation of nonlinear SAWs in the (111) surface cut for a variety of cubic crystals. The SAWs in this plane differ from those in the (001) surface cut in that the nonlinearity matrix elements cannot usually be written in real-valued form. The nonlinearity matrix elements have sixfold symmetry in magnitude but only threefold symmetry in phase. In most directions, initially sinusoidal waveforms distort asymmetrically and, in some cases, the dissimilar phases of the nonlinearity matrix elements result in oscillations forming in the vicinity of the shocks and peaks of the velocity waveforms. Detailed analysis is provided for Si and KCl. A simple mathematical transformation is introduced to provide a graphical interpretation of the phase information contained in the nonlinearity matrix elements and linear amplitude factors. Comparisons are made between waveforms approximated by this method and those generated with the full simulation. The agreement is shown to be best when most of the nonlinearity matrix elements of the crystals have the same or approximately the same phase. By this approach, plots of the nonlinearity matrix elements as a function of direction can be used to characterize the types of harmonic generation and waveform distortion in some directions. The analysis provided here is applicable to other crystals and surface cuts as well, such as in the (110) surface cut of cubic crystals in the $m\bar{3}$ point symmetry group.

ACKNOWLEDGMENTS

This work was supported by the Office of Naval Research. We also gratefully acknowledge discussions with Yu. A. Ilinskii and E. A. Zabolotskaya at The University of Texas at Austin, and P. Hess and A. Lomonosov at the University of Heidelberg, Germany.

[1] R. E. Kumon and M. F. Hamilton, ''Directional dependence of nonlinear surface acoustic waves in the (001) plane of cubic crystals,'' J. Acoust. Soc. Am. **111**, 2060–2069 (2002).

[2] M. F. Hamilton, Yu. A. Il'inskii, and E. A. Zabolotskaya, ''Nonlinear surface acoustic waves in crystals,'' J. Acoust. Soc. Am. **105**, 639–651 (1999).

[3] R. E. Kumon, M. F. Hamilton, Yu. A. Il'inskii, E. A. Zabolotskaya, P. Hess, A. Lomonosov, and V. G. Mikhalevich, ''Pulsed nonlinear surface acoustic waves in crystals,'' in *Proceedings of the 16th International Congress on Acoustics and 135th Meeting of the Acoustical Society of America*, edited by P. K. Kuhl and L. A. Crum (Acoustical Society of America, Woodbury, NY, 1998), Vol. 3, pp. 1557–1558.

[4] M. F. Hamilton, Yu. A. Il'insky, and E. A. Zabolotskaya, ''Local and nonlocal nonlinearity in Rayleigh waves,'' J. Acoust. Soc. Am. **97**, 882–890 (1995).

[5] E. Yu. Knight, M. F. Hamilton, Yu. A. Il'inskii, and E. A. Zabolotskaya, ''On Rayleigh wave nonlinearity, and analytical approximation of the shock formation distance,'' J. Acoust. Soc. Am. **102**, 2529–2535 (1997).

[6] E. A. Zabolotskaya, ''Nonlinear propagation of plane and circular Rayleigh waves,'' J. Acoust. Soc. Am. **91**, 2569–2575 (1992).

[7] G. W. Farnell, ''Properties of elastic surface waves,'' in *Physical Acoustics*, edited by W. P. Mason and R. N. Thurston (Academic, New York, 1970), Vol. 6, pp. 109–166.

[8] A. Lomonosov, P. Hess, R. E. Kumon, and M. F. Hamilton, ''Periodicity of linear and nonlinear surface acoustic wave parameters in the (111) plane of cubic crystals,'' J. Acoust. Soc. Am. **110**, 2702(A) (2001).

[9] G. D. Meegan, M. F. Hamilton, Yu. A. Il'inskii, and E. A. Zabolotskaya, ''Nonlinear Stoneley and Scholte waves,'' J. Acoust. Soc. Am. **106**, 1712–1723 (1999).

[10] D. J. Shull, M. F. Hamilton, Yu. A. Il'insky, and E. A. Zabolotskaya, ''Harmonic generation in plane and cylindrical nonlinear Rayleigh waves,'' J. Acoust. Soc. Am. **94**, 418–427 (1993).

[11] A. Lomonosov, V. G. Mikhalevich, P. Hess, E. Yu. Knight, M. F. Hamilton, and E. A. Zabolotskaya, ''Laser-generated nonlinear Rayleigh waves with shocks,'' J. Acoust. Soc. Am. **105**, 2093–2096 (1999).

[12] R. E. Kumon, ''Nonlinear surface acoustic waves in cubic crystals,'' Ph.D. dissertation, The University of Texas at Austin, 1999.

[13] L. K. Zarembo and V. A. Krasil'nikov, ''Nonlinear phenomena in the propagation of elastic waves in solids,'' Sov. Phys. Usp. **13**, 778–797 (1971).

[14] R. N. Bracewell, *The Fourier Transform and Its Applications*, 2nd ed. (McGraw–Hill, New York, 1978).

[15] W. Borchardt-Ott, *Crystallography*, 2nd ed. (Springer-Verlag, New York, 1995).